Purkinje neuron Ca^{2+} influx reduction rescues ataxia in SCA28 model

Francesca Maltecca,[1] Elisa Baseggio,[1] Francesco Consolato,[1] Davide Mazza,[2] Paola Podini,[3] Samuel M. Young Jr.,[4] Ilaria Drago,[5,6] Ben A. Bahr,[7] Aldamaria Puliti,[8] Franca Codazzi,[9] Angelo Quattrini,[3] and Giorgio Casari[1]

[1]Università Vita-Salute San Raffaele and Division of Genetics and Cell Biology, [2]Università Vita-Salute San Raffaele and Experimental Imaging Center, and [3]Institute of Experimental Neurology, Division of Neuroscience, San Raffaele Scientific Institute, Milan, Italy. [4]Research Group for Molecular Mechanisms of Synaptic Function, Max Planck Florida Institute for Neuroscience, Jupiter, Florida, USA. [5]Department of Biomedical Sciences, University of Padua, Padua, Italy. [6]Department of Neuroscience, The Scripps Research Institute Florida, Jupiter, Florida, USA. [7]Biotechnology Research and Training Center, University of North Carolina-Pembroke, Pembroke, North Carolina, USA. [8]Medical Genetics Unit, Istituto Giannina Gaslini, Genoa, Italy, and Department of Neurosciences, Rehabilitation, Ophthalmology, Genetics, Maternal and Child Health (DiNOGMI), University of Genoa, Genoa, Italy. [9]Cellular Neurophysiology Unit, Division of Neuroscience, San Raffaele Scientific Institute, Milan, Italy.

Spinocerebellar ataxia type 28 (SCA28) is a neurodegenerative disease caused by mutations of the mitochondrial protease AFG3L2. The SCA28 mouse model, which is haploinsufficient for *Afg3l2*, exhibits a progressive decline in motor function and displays dark degeneration of Purkinje cells (PC-DCD) of mitochondrial origin. Here, we determined that mitochondria in cultured *Afg3l2*-deficient PCs ineffectively buffer evoked Ca^{2+} peaks, resulting in enhanced cytoplasmic Ca^{2+} concentrations, which subsequently triggers PC-DCD. This Ca^{2+}-handling defect is the result of negative synergism between mitochondrial depolarization and altered organelle trafficking to PC dendrites in *Afg3l2*-mutant cells. In SCA28 mice, partial genetic silencing of the metabotropic glutamate receptor mGluR1 decreased Ca^{2+} influx in PCs and reversed the ataxic phenotype. Moreover, administration of the β-lactam antibiotic ceftriaxone, which promotes synaptic glutamate clearance, thereby reducing Ca^{2+} influx, improved ataxia-associated phenotypes in SCA28 mice when given either prior to or after symptom onset. Together, the results of this study indicate that ineffective mitochondrial Ca^{2+} handling in PCs underlies SCA28 pathogenesis and suggest that strategies that lower glutamate stimulation of PCs should be further explored as a potential treatment for SCA28 patients.

Introduction

SCA28 is a form of dominant cerebellar ataxia characterized by unbalanced standing, gait incoordination, hyperreflexia of the lower limbs, nystagmus, and ophthalmoparesis (1). Several SCA28-causing missense mutations have been identified in the *AFG3L2* gene (2–4). Moreover, homozygous mutations in *AFG3L2* are responsible for a myoclonic epilepsy-ataxia-polyneuropathy syndrome of childhood (5).

SCA28 is the first autosomal dominant spinocerebellar ataxia (SCA) to be caused by alterations in a mitochondrial protein. Indeed, AFG3L2 belongs to the AAA (ATPases associated with various cellular activities) protease superfamily and assembles with paraplegin in the inner mitochondrial membrane into homo-oligomers and hetero-oligomers, named *m*-AAA proteases. The *m*-AAA complexes are crucial components of the quality-control system in the inner membrane, where they mediate the selective degradation of nonassembled and damaged proteins (6). In addition, they exert chaperone-like activity on respiratory chain complexes (7–9) and regulate the processing of the profusion protein OPA1 (10–13) and the subunit of mitochondrial ribosomes MRPL32 (14).

Most of the reported SCA28-causing mutations are heterozygous loss-of-function mutations clustering within the proteolytic domain of AFG3L2. Several pieces of evidence support the hypothesis that haploinsufficiency is the SCA28-causing mechanism. First, functional studies of human mutant AFG3L2 expression in the *m*-AAA–deficient yeast strain indicate that SCA28 mutations alter the proteolytic competence of AFG3L2 and result in impaired respiration. However, the coexpression of WT and mutant AFG3L2 is able to correct the respiratory defect for most of the mutations, indicating that haploinsufficiency is the disease-causing mechanism (2). Remarkably, a partial AFG3L2 deletion (exons 14–16) has been recently identified as the cause of SCA28 in 2 large Belgian families, and functional studies revealed a reduced number of *m*-AAA complexes in these patients, demonstrating that SCA28 is due to haploinsufficiency (15). Indeed, the *Afg3l2*-haploinsufficient mouse resembles the phenotype of SCA28 patients, showing a progressive decline in motor performance caused by dark degeneration of Purkinje cells (PC-DCD) (16). The latter is a specific form of a cell degeneration intermediate between necrosis and apoptosis and is characterized by cell shrinkage, cytoplasm darkening, and chromatin condensation (17). In the SCA28 mouse, this phenomenon is unique, since it originates from mitochondrial dysfunction (16), while in other forms of SCA, it is associated with excitotoxicity and high levels of intracellular Ca^{2+} (18–20).

Note regarding evaluation of this manuscript: Manuscripts authored by scientists associated with Duke University, The University of North Carolina at Chapel Hill, Duke-NUS, and the Sanford-Burnham Medical Research Institute are handled not by members of the editorial board but rather by the science editors, who consult with selected external editors and reviewers.

Conflict of interest: The authors declare that no conflict of interest exists.

Submitted: December 13, 2013; **Accepted:** November 6, 2014.

Reference information: *J Clin Invest*. doi:10.1172/JCI74770.

PCs are some of the largest and most complex neurons of the mammalian CNS. They present extremely branched dendritic trees with a large number of active spines, which uniquely receive glutamatergic stimulation of ionotropic α-amino-3-hydroxy-5-methyl-4-isoxazolepropionic acid (AMPA) receptors and metabotropic receptors (e.g., mGluR1) as afferent inputs. PCs are therefore exposed to massive and sudden Ca^{2+} influx and are especially vulnerable to glutamate-mediated excitotoxicity (21). To control Ca^{2+} homeostasis, PCs take advantage of several Ca^{2+} clearance systems: the Ca^{2+} ATPase and the Ca^{2+}-Na^{+} exchanger at the plasma membrane, the Ca^{2+} ATPase at the ER, and Ca^{2+}-binding proteins (22).

Mitochondria accumulate Ca^{2+} in the matrix via the low-affinity mitochondrial Ca^{2+} uniporter (MCU) in a process that depends on the electrical potential across the inner membrane ($\Delta\psi_{mito}$) (23). While the capability of mitochondria to internalize Ca^{2+} is undisputed, their functional role in living cells, and especially in neurons, is less clear. Compelling evidence indicates that mitochondria can act as local Ca^{2+} buffers in different neuronal cell types (24–26), but the effective impact of this process on neuronal Ca^{2+} homeostasis and physiology remains to be clarified.

The efficacy of mitochondrial Ca^{2+} uptake is strictly dependent on the proximity of the organelles to the Ca^{2+} source (e.g., ER, plasma membrane, dendritic spines) (23, 27). Neurons are therefore particularly reliant on proper trafficking of mitochondria to these sites and consequently on their dynamic properties. Mitochondria continuously fuse and fragment to mix lipids and matrix content and are also actively recruited to subcellular sites, such as the axonal and dendritic processes. Defects in these key features are indeed associated with neurodegenerative diseases (28). Also, alterations in both fusion and fission have been shown to decrease mitochondrial movement (29). Interestingly, loss of AFG3L2 results in increased organellar fragmentation due to enhanced processing of OPA1 (12, 16).

In this study, we have dissected the pathogenetic mechanism of SCA28 in primary PC neurons and provide the first evidence to our knowledge of a pharmacological treatment for this disease in preclinical models. Indeed, we have demonstrated in cultured PCs that *Afg3l2* depletion causes defective Ca^{2+} uptake by mitochondria. The inefficient buffering and shaping of Ca^{2+} peaks by mutant mitochondria provoke an increase in cytoplasmic Ca^{2+} concentrations ($[Ca^{2+}]_{cyto}$), thus triggering PC-DCD. The impaired mitochondrial Ca^{2+} buffering results from the negative synergism of both depolarization of mitochondria and alteration of the mitochondrial morphology, which also hamper the proper trafficking of the organelles into dendrites.

As a proof of principle of this pathogenetic mechanism, we show that half dosage of mGluR1 (and thus reduced Ca^{2+} influx into PCs) completely reverses both motor impairment and PC-DCD in *Afg3l2*$^{+/-}$ mice.

Finally, we obtained the same result by pharmacological treatment with ceftriaxone, an antibiotic able to increase expression of the astrocyte glutamate transporter EAAT2, thereby lowering the glutamatergic stimulation of PCs.

Results

Afg3l2 depletion in PCs leads to increased susceptibility to high Ca^{2+} concentrations. In *Afg3l2*$^{+/-}$ mice, PCs present morphological features typical of DCD (Figure 1A). DCD in this model represents approximately 20% to 30% of PCs at 8 months, as already reported (16). This phenomenon is caused by an increase in $[Ca^{2+}]_{cyto}$, thus activating calpains, which are Ca^{2+}-sensitive cysteine proteases that mediate cytoskeletal breakdown (30–32). Looking for molecular evidence of activation of this pathway in SCA28, we assayed calpain-mediated proteolysis of αII-spectrin, which was expected to result in 2 proteolytic fragments of nearly equal electrophoretic mobility (~150 kDa) (33). These fragments were indeed found in the cerebellum of *Afg3l2*$^{+/-}$ mice by Western blot (WB) analysis and comigrated with the fragments obtained by treating WT cerebellar extracts with recombinant m-calpain plus 2 mM Ca^{2+}, thus demonstrating increased $[Ca^{2+}]_{cyto}$ and calpain activation (Figure 1, B and C).

We then investigated whether PCs in which *Afg3l2* expression is reduced or abolished are selectively susceptible to stimuli that increase $[Ca^{2+}]_{cyto}$. To this end, we used cerebellar sections from *Afg3l2*-depleted mice and WT littermates and elicited DCDs by a brief exposure to AMPA (34). In fact, PCs express high levels of AMPA receptors, whose activation is able to increase $[Ca^{2+}]_{cyto}$ (21). Upon AMPA treatment, we found that the number of PC-DCDs (identified by immunofluorescence [IF] using an Ab that specifically recognizes the amino-terminal breakdown product of calpain-cleaved spectrin; ref. 30), was increased in *Afg3l2*$^{+/-}$ PCs compared with the number in WT PCs, and this effect was even greater in *Afg3l2*$^{-/-}$ cells (Figure 1, D and E, and Supplemental Figure 1), supporting a higher susceptibility of *Afg3l2*-depleted PCs to stimuli that increase $[Ca^{2+}]_{cyto}$. We obtained the same result by performing WB analysis of cerebellar slices using an Ab against spectrin (Figure 1B), which revealed an increased amount of cleaved spectrin in *Afg3l2*$^{-/-}$ and *Afg3l2*$^{+/-}$ PCs compared with that detected in WT slices (Figure 1F).

Loss of Afg3l2 in PCs results in reduced mitochondrial Ca^{2+} uptake and increased cytosolic Ca^{2+} concentration. In the SCA28 mouse, PC-DCD originates from mitochondrial dysfunction (16). Since PCs are exposed to massive Ca^{2+} influx (21) and mitochondria can transiently store large amounts of Ca^{2+} (23, 27), we reasoned that defective Ca^{2+} buffering operated by *Afg3l2*-mutant mitochondria in PCs could increase $[Ca^{2+}]_{cyto}$ and cause DCD, thus mimicking excitotoxicity. This hypothesis was also supported by our previous data showing reduced $[Ca^{2+}]$ in the mitochondrial matrix of *Afg3l2*-depleted fibroblasts (13).

To address this issue, we decided to measure (a) mitochondrial $[Ca^{2+}]$ ($[Ca^{2+}]_{mito}$), and (b) $[Ca^{2+}]_{cyto}$ in primary cerebellar cultures from *Afg3l2*-depleted mice. In these cultures PCs are present together with other cerebellar neurons (mainly granule cells) and Bergmann glia (Supplemental Figure 2A), which are required for PC survival and function (35). We first performed a quantitative evaluation of PC morphology by IF using anti-calbindin Ab at day 14 in vitro (14 DIV). *Afg3l2*$^{+/-}$ PCs appeared comparable to those in WT mice, while in *Afg3l2*$^{-/-}$ PCs, we found that dendrites were slightly decreased in number and length (Supplemental Figure 2, B and C), but were considerably reduced in terms of area, appearing thinner with shorter side branches (Figure 2, A and B). Spines were visible in the dendrites of PCs of each genotype, with no significant differences in spine density (Supplemental Figure 2D). We also verified that PCs correctly expressed mGluR1 receptors (Supplemental Figure 2A).

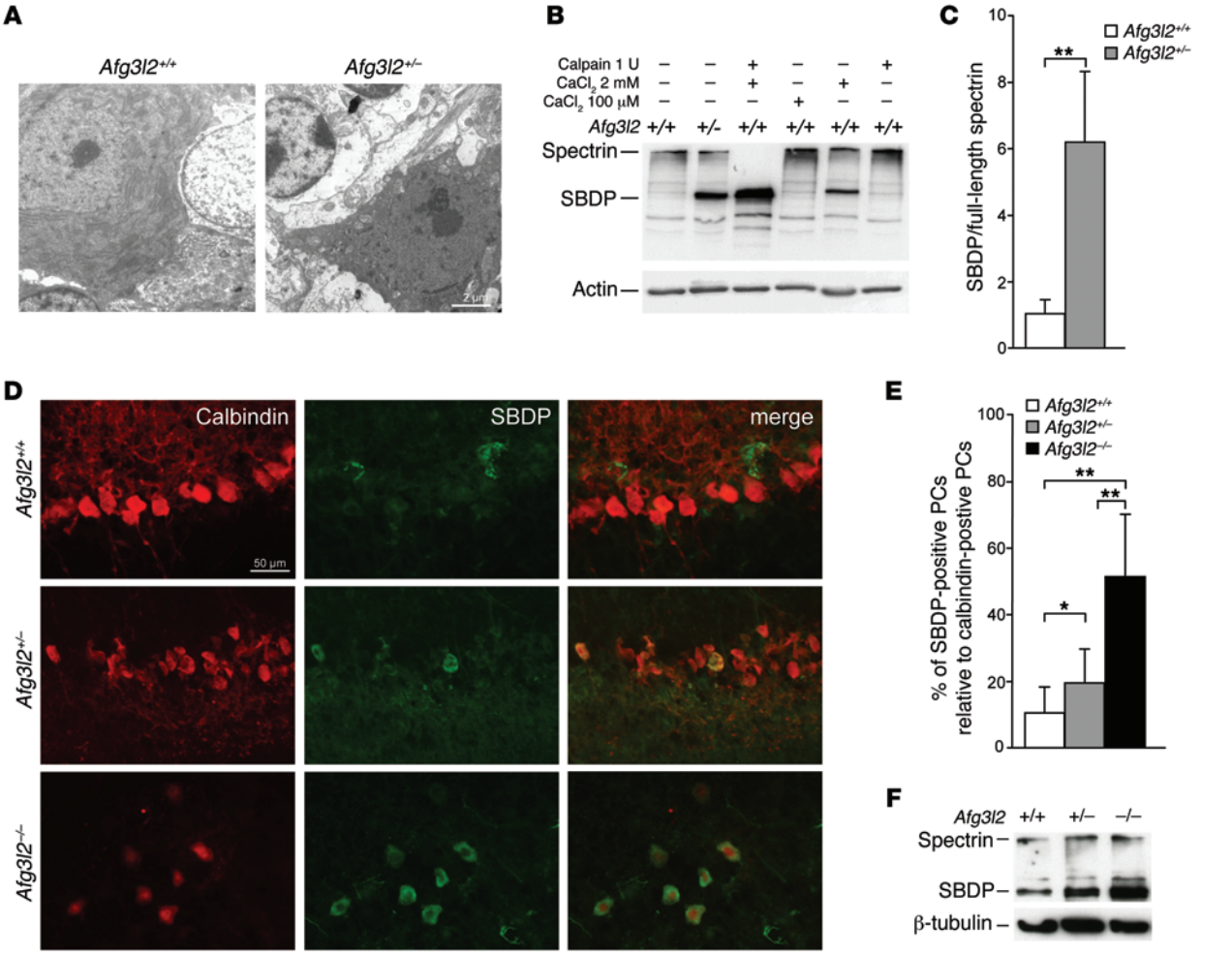

Figure 1. Reduced dosage of AFG3L2 in PCs induces dark degeneration. (**A**) Ultrathin sections of cerebella from 6-month-old *Afg3l2*$^{+/-}$ and WT mice showing dark degeneration of PCs. Scale bar: 2 μm. (**B**) WB analysis of cerebellar extracts from *Afg3l2*$^{+/-}$ and WT mice. When indicated, $CaCl_2$ and/or 1 U calpain were added. (**C**) Densitometric analysis of WB bands. Data represent the mean ± SD; $n = 3$; $^{**}P < 0.001$ by Student's t test. (**D**) IF images of organotypic cerebellar slices obtained from 10-day-old *Afg3l2*$^{-/-}$ and *Afg3l2*$^{+/-}$ mice and their WT littermates after AMPA exposure. Abs against calbindin and SBDPs were used. Scale bar: 50 μm. (**E**) Quantitative evaluation of dark-degenerated (SBDP-positive) PCs relative to the total number of PCs in cerebellar slices treated with AMPA. Data represent the mean ± SD; $n = 4$, with an average of 25 neurons analyzed per genotype per experiment. $^{*}P < 0.05$ and $^{**}P < 0.001$ by Student's t test. (**F**) WB analysis of cerebellar slices revealing an increased amount of SBDPs in *Afg3l2*$^{-/-}$ and *Afg3l2*$^{+/-}$ mice compared with that detected in WT mice.

To measure $[Ca^{2+}]_{mito}$ in PCs in primary cerebellar cultures, we created an adeno-associated viral vector expressing a mitochondria-targeted version of the GFP-based Ca^{2+} probe 4mtD1cpv (36) under the synapsin promoter. Transduction of this probe in primary cerebellar cultures gave a neuron-specific signal. Among the various neuronal types, PCs were easily distinguished in bright-field, as they were markedly larger and more ramified than granule cells. Upon challenge with 30 mM KCl, which depolarizes the plasma membrane in neurons by opening potential-sensitive Ca^{2+} channels, we observed that mitochondrial Ca^{2+} rises of transduced neurons were significantly smaller in *Afg3l2*$^{-/-}$ PCs compared with those in *Afg3l2*$^{+/-}$ and WT cells (Figure 2, C and D).

In parallel, we performed ratiometric measurement of $[Ca^{2+}]_{cyto}$ in PCs by using the high-affinity Ca^{2+} indicator fura-2. We found that the basal levels of $[Ca^{2+}]_{cyto}$ were identical in the 3 genotypes (Figure 2E). In contrast, we observed that in *Afg3l2*$^{-/-}$ PCs, the peak Ca^{2+} response elicited by acute exposure to 30 mM KCl was significantly higher than that in *Afg3l2*$^{+/-}$ and WT PCs (Figure 2F). Of note, the peak Ca^{2+} response observed in *Afg3l2*$^{-/-}$ PCs was comparable to that measured by pretreating WT PCs with the respiratory chain uncoupler trifluorocarbonylcyanide phenylhydrazone (FCCP) (Figure 2F). Our analysis of the decay kinetics revealed no significant differences among the genotypes, demonstrating that active Ca^{2+} clearance systems of mutant PCs (e.g., plasma membrane Ca^{2+} ATPase and ER Ca^{2+} ATPase) were unaffected (Figure 2, G and H).

We verified that an increased Ca^{2+} response in the absence of AFG3L2 in PCs occurs not only in the presence of a depolarizing stimulus such as KCl, but also in the presence of the group I mGluR agonist (*S*)-3,5-dihydroxyphenylglycine (DHPG), which is capable of inducing Ca^{2+} release from the ER (21). We first confirmed the absence of a Ca^{2+} response in primary PCs lacking mGluR1 (Supplemental Figure 3, A and B). We then treated *Afg3l2*$^{-/-}$ and WT

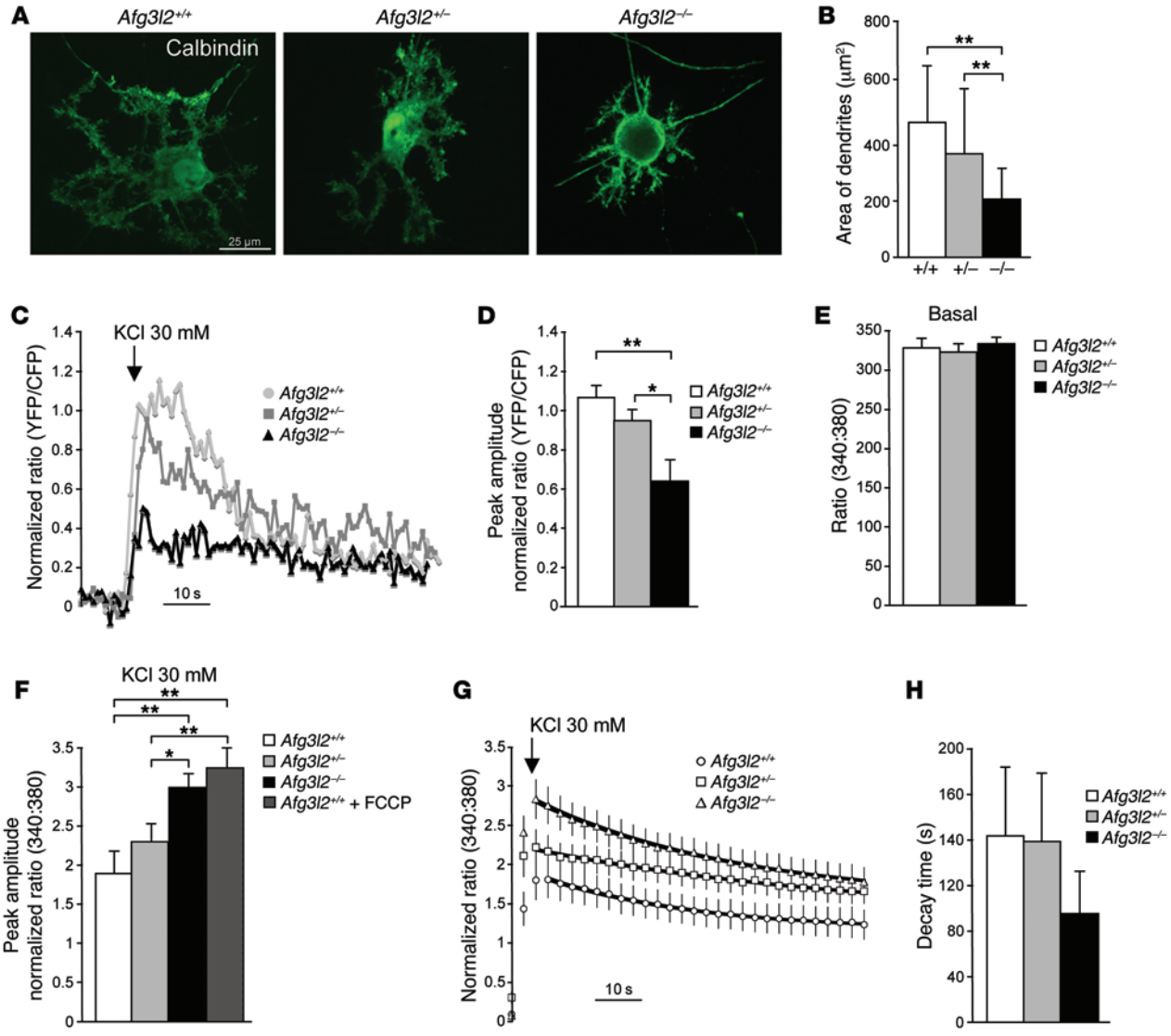

Figure 2. Reduced mitochondrial Ca^{2+} uptake in the absence of AFG3L2 results in increased $[Ca^{2+}]_{cyto}$. (**A**) IF images of primary PCs at 14 DIV using anti-calbindin Ab. (**B**) Quantification of the area of dendrites. Data represent the mean ± SD; $n = 6$, with ~20 neurons analyzed per experiment. $^{**}P < 0.001$ by Student's t test. (**C**) Representative traces of evoked $[Ca^{2+}]_{mito}$ responses in PCs expressing 4mtD1cpv. (**D**) Mean ± SEM of peak $[Ca^{2+}]_{mito}$ responses after KCl stimulation (normalized increase in the YFP/CFP fluorescence ratio measured above the initial value. $n = 4$, with ~20 traces analyzed per experiment. $^{*}P < 0.05$ and $^{**}P < 0.001$ by Student's t test. (**E**) Basal values of $[Ca^{2+}]_{cyto}$ evaluated by fura-2 fluorescence at a 340:380 nm ratio. Data represent the mean ± SEM; $n = 5$, with ~10 traces analyzed per experiment. (**F**) Mean ± SEM of peak $[Ca^{2+}]_{cyto}$ responses after stimulation with 30 mM KCl (normalized increase measured above the initial value; $n = 5$, with ~15 traces analyzed per experiment). $^{*}P < 0.05$ and $^{**}P < 0.001$ by Student's t test. (**G**) Average traces of $[Ca^{2+}]_{cyto}$ responses before and after KCl stimulation. Decays following the peak response were fit with a single exponential (black lines). (**H**) Mean ± SEM of the decay times measured for each trace of $[Ca^{2+}]_{cyto}$ as obtained by fitting the individual traces with an exponential decay. $n = 5$, with ~15 traces analyzed per experiment.

PCs with DHPG, which elicited an increased peak Ca^{2+} response in *Afg3l2*$^{-/-}$ cells compared with that seen in WT cells (Supplemental Figure 3C, Supplemental Results, and Supplemental Methods), in agreement with what we showed in Figure 2F after the administration of a depolarizing stimulus that enhanced Ca^{2+} influx into the cell from the plasma membrane. This result demonstrates that the inefficient mitochondrial Ca^{2+} buffering in *Afg3l2*$^{-/-}$ PCs causes abnormal cytosolic Ca^{2+} elevation, even in the presence of a stimulus inducing Ca^{2+} release from the ER.

Loss of Afg3l2 in primary PCs induces mitochondrial morphological alterations and depletion of dendritic mitochondria. To understand the molecular basis of the decreased mitochondrial Ca^{2+} buffering in *Afg3l2*-depleted PCs, we examined the morphology, distribution, and metabolic status of mitochondria in primary PCs.

We first performed IF and confocal microscopy using an Ab against both COX1 (mitochondrial marker) and calbindin (PC marker). In *Afg3l2*$^{-/-}$ PCs, mitochondria were mostly round shaped, as was previously observed in MEFs (13), in contrast to the tubular-shaped organelles we observed in syngenic controls (Figure 3A). We also investigated whether alterations of mitochondrial morphology alter the trafficking of organelles to the distal dendritic branches of PCs. Using 3D reconstruction of confocal stacks

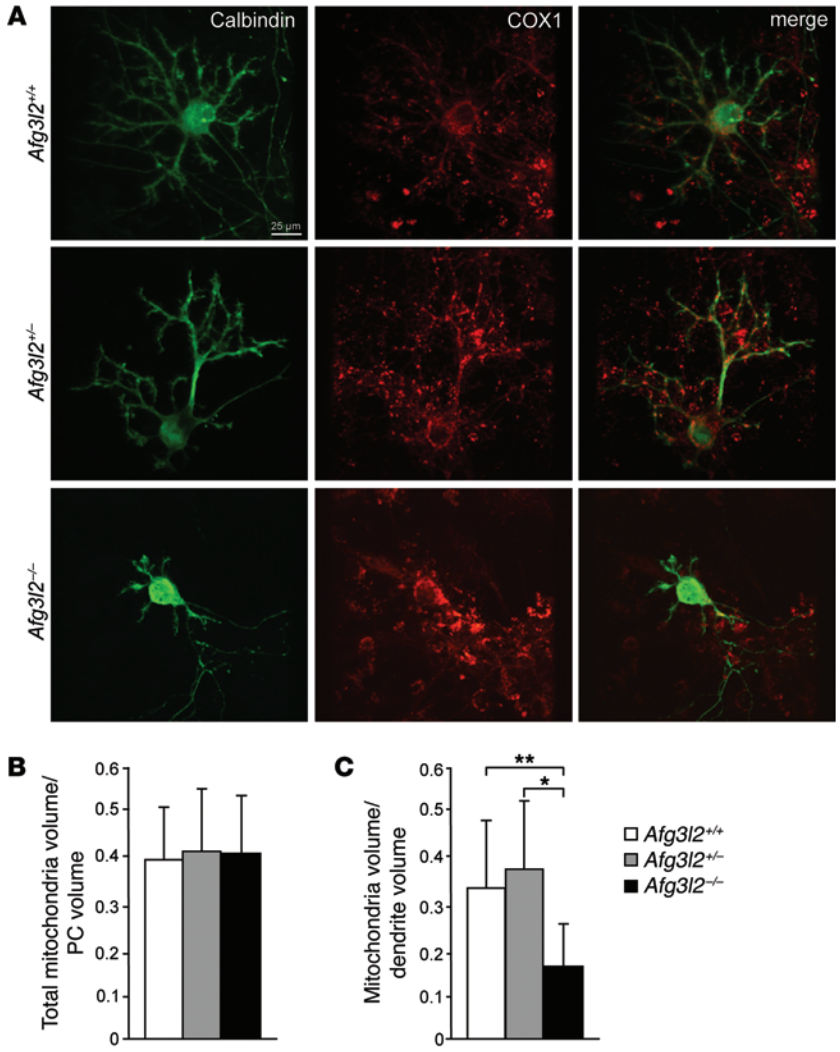

Figure 3. Loss of Afg3l2 in PCs alters dendritic mitochondrial content. (**A**) IF images of primary PCs from the indicated genotypes at 14 DIV using Ab against the PC marker calbindin and the mitochondrial marker COX1 analyzed by confocal imaging. Scale bar: 25 μm. (**B** and **C**) Quantification of total mitochondria volume relative to total PC volume (**B**) or relative to PC dendrite volume (**C**) analyzed by 3D reconstruction of consecutive confocal stacks taken at 0.3 μm. $n = 15$ PCs analyzed per genotype. $^*P < 0.05$ and $^{**}P < 0.001$ by Student's t test.

of PCs stained with anti-calbindin and anti-COX1 Ab, we analyzed the volume of mitochondria in the whole PC volume and in dendrites. We observed no change in total mitochondrial volume in *Afg3l2*$^{-/-}$ PCs, though these cells contained fewer mitochondria in their dendrites, indicating an accumulation of organelles in the soma (Figure 3, B and C).

Alteration of cristae morphology correlates with mitochondrial depolarization in Afg3l2-depleted PCs. To further address the defective trafficking of mitochondria, we assayed the mitochondrial ultrastructure by electron microscopy (EM). In WT PCs, we observed that mitochondria were evenly distributed in the cell soma and dendrites, had structurally intact inner and outer membranes with well-defined cristae, and were tubular in shape. In contrast, in *Afg3l2*$^{+/-}$ PCs, we observed a remodeling of the inner membrane conformation, ranging from widening to vesiculation of the cristae, which worsened dramatically in *Afg3l2*$^{-/-}$ PCs, in which most of the organelles appeared swollen (Figure 4A). Quantification of these alterations is reported in Figure 4B. Consistent with our confocal microscopic observations, in *Afg3l2*$^{-/-}$ PCs, mitochondria aggregated in the soma, leaving dendrites depleted of organelles. We detected no differences in mitochondrial distribution between *Afg3l2*$^{+/-}$ and WT PC dendrites, indicating that organellar morphological alterations in the heterozygous mice may not be severe enough to hamper entry of the organelles into the dendritic tree, at least in culture conditions.

These data prompted us to evaluate the metabolic status of the organelles in *Afg3l2*-depleted conditions. We therefore tested $\Delta\psi_{mito}$ by live-imaging measurement of the potentiometric dye tetramethylrhodamine methyl ester (TMRM) in primary PCs. In *Afg3l2*$^{+/-}$ PCs, and to a greater extent in *Afg3l2*$^{-/-}$ PCs, we observed a depolarization of mitochondria in the soma that was even more pronounced in dendrites (Figure 4C), indicating that PC mitochondria lacking AFG3L2 or with a halved dosage of AFG3L2 are metabolically dysfunctional.

Reduced excitatory stimulation of PCs rescues the ataxic phenotype of Afg3l2$^{+/-}$ *mice.* Considering these pieces of evidence, we designed a rescue strategy based on the rationale that reducing Ca^{2+} influx into PCs by lowering their glutamatergic stimulation could prevent, or at least ameliorate, the cerebellar phenotype of SCA28 mutants. We addressed this goal using a binary approach, i.e., a genetic and pharmacological rescue.

Activation of the mGluR1 receptor is linked to IP3-mediated Ca^{2+} release from the ER (21). We thus crossed *Afg3l2*-haploinsufficient mice with cervelet-4 (*crv4*) heterozygous mice, which carry a spontaneous mutation causing loss of function of mGluR1 encoded by the *Grm1* gene (37). We first verified a halved amount of the mGluR1 receptor (Supplemental Figure 4A) and excluded increased levels of AMPA receptors (Supplemental Figure 4B), signs of gait ataxia and cerebellar morphological alterations in *Grm1*$^{+/crv4}$ mice (Supplemental Figure 4, C and D). Also, we found no mGluR5 expression in adult PCs in either WT or *Grm1*$^{+/crv4}$ mice (Supplemental Figure 4E).

In agreement with the proposed mechanism of pathogenesis, we demonstrated that the SCA28 phenotype is fully rescued by halving the amount of the mGluR1 receptor and thus reducing the release of Ca^{2+} from the ER. Indeed, the *Afg3l2*$^{+/-}$ *Grm1*$^{+/crv4}$ double mutants displayed motor function and coordination within the normal range, as demonstrated by beam-walking tests (Figure 5A and Supplemental Videos 1 and 2). Accordingly, neuropathological examination indicated that rescue of the ataxic phenotype correlated with decreased PC-DCD in *Afg3l2*$^{+/-}$ *Grm1*$^{+/crv4}$

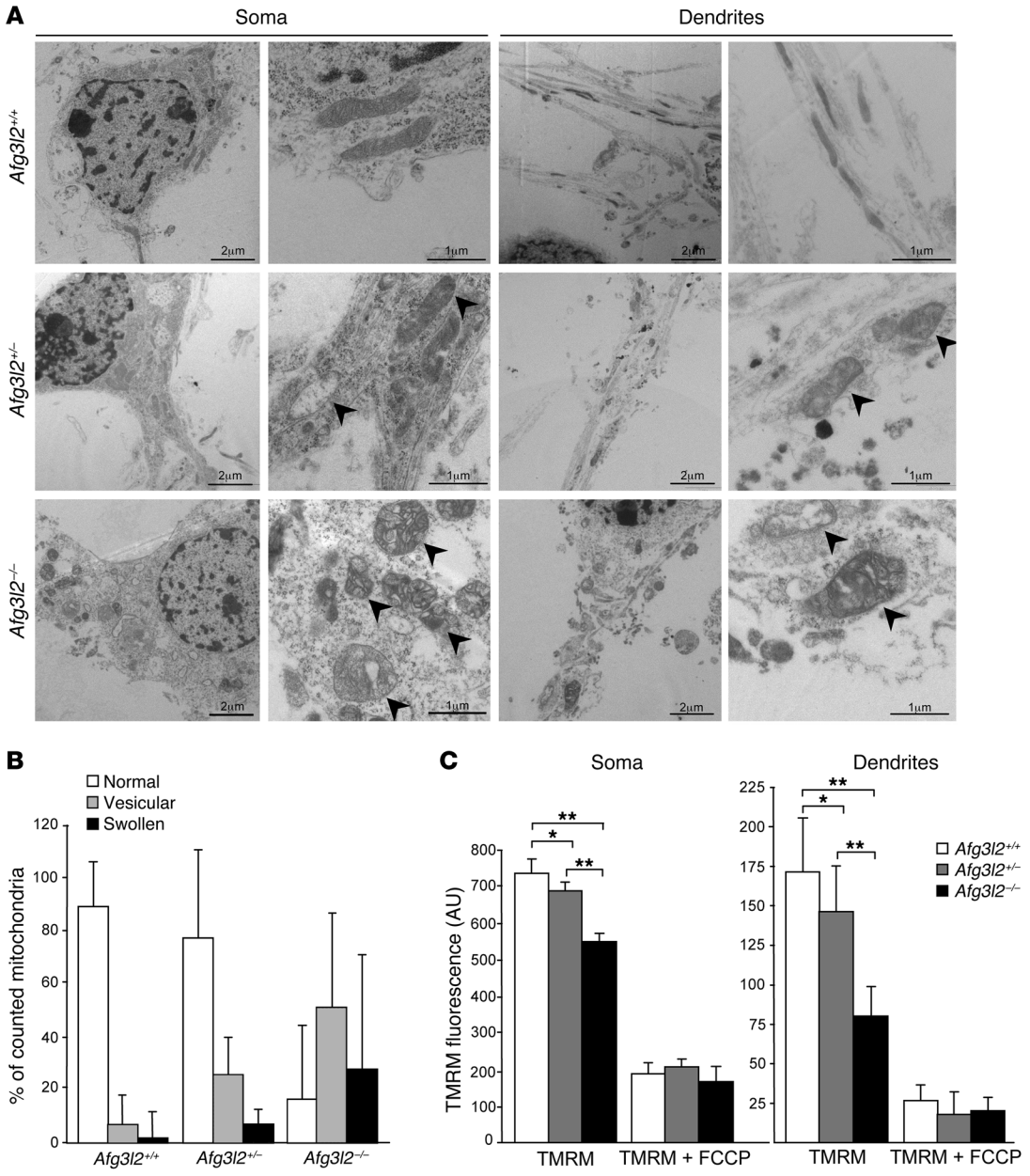

Figure 4. Afg3l2 depletion in PCs causes dramatic changes in mitochondrial ultrastructure and reduced membrane potential. (**A**) EM of primary PCs at 14 DIV. Arrowheads indicate aberrant mitochondria. Scale bars: 2 μm (left panels, soma and dendrites); 1 μm (right panels, soma and dendrites). (**B**) Quantification of mitochondrial ultrastructural alterations. Organelles were classified as normal, vesicular, or swollen on the basis of inner membrane remodeling. Graph indicates the mean ± SD of an average of 200 mitochondria from 5 cells in 3 independent experiments. χ^2 test (2 degrees of freedom): *Afg3l2*$^{-/-}$ versus either *Afg3l2*$^{+/-}$ or WT PCs, $P < 0.001$, WT versus *Afg3l2*$^{+/-}$, $P < 0.05$. (**C**) Analysis of $\Delta\psi_{mito}$ in primary PCs by live-imaging measurement of TMRM fluorescence intensity in soma and dendrites, respectively. Data represent the mean ± SEM; $n = 5$, with an average of 40 cells analyzed per experiment. At the end of the experiments, 1 μM FCCP was added. *$P < 0.05$ and **$P < 0.001$ by Student's t test.

versus *Afg3l2*$^{+/-}$ mice (Figure 5, B–E). The molecular link between decreased PC-DCD and lower Ca^{2+} peaks was complemented by in vitro experiments, which disclosed a significant reduction in peak Ca^{2+} responses in *Afg3l2*$^{-/-}$ *Grm1*$^{+/crv4}$ versus *Afg3l2*$^{-/-}$ primary PCs after DHPG stimulation (Supplemental Figure 3C), strongly indicating that mGluR1 haploinsufficiency is protective and able to prevent the exacerbation of glutamate stimulation in *Afg3l2*$^{-/-}$ PCs.

In order to test the rescue of the ataxic phenotype by drug treatment, *Afg3l2*$^{+/-}$ mice were administered the β-lactam antibiotic ceftriaxone, which is capable of increasing EAAT2 expression and activity (38). We used this drug to specifically reduce postsynaptic glutamatergic stimulation of PCs in *Afg3l2*$^{+/-}$ mice, and thus Ca^{2+} influx. We first determined that EAAT2-increased expression was maintained for approximately 7 to 8 weeks in the cerebellum after ceftriaxone treatment (Supplemental Figure 5A). We thus treated *Afg3l2*$^{+/-}$ and WT mice at 3 months of age (about 1 month before the onset of motor impairment; ref. 16) and repeated the treatment 2 months later. We observed that ceftriaxone adminis-

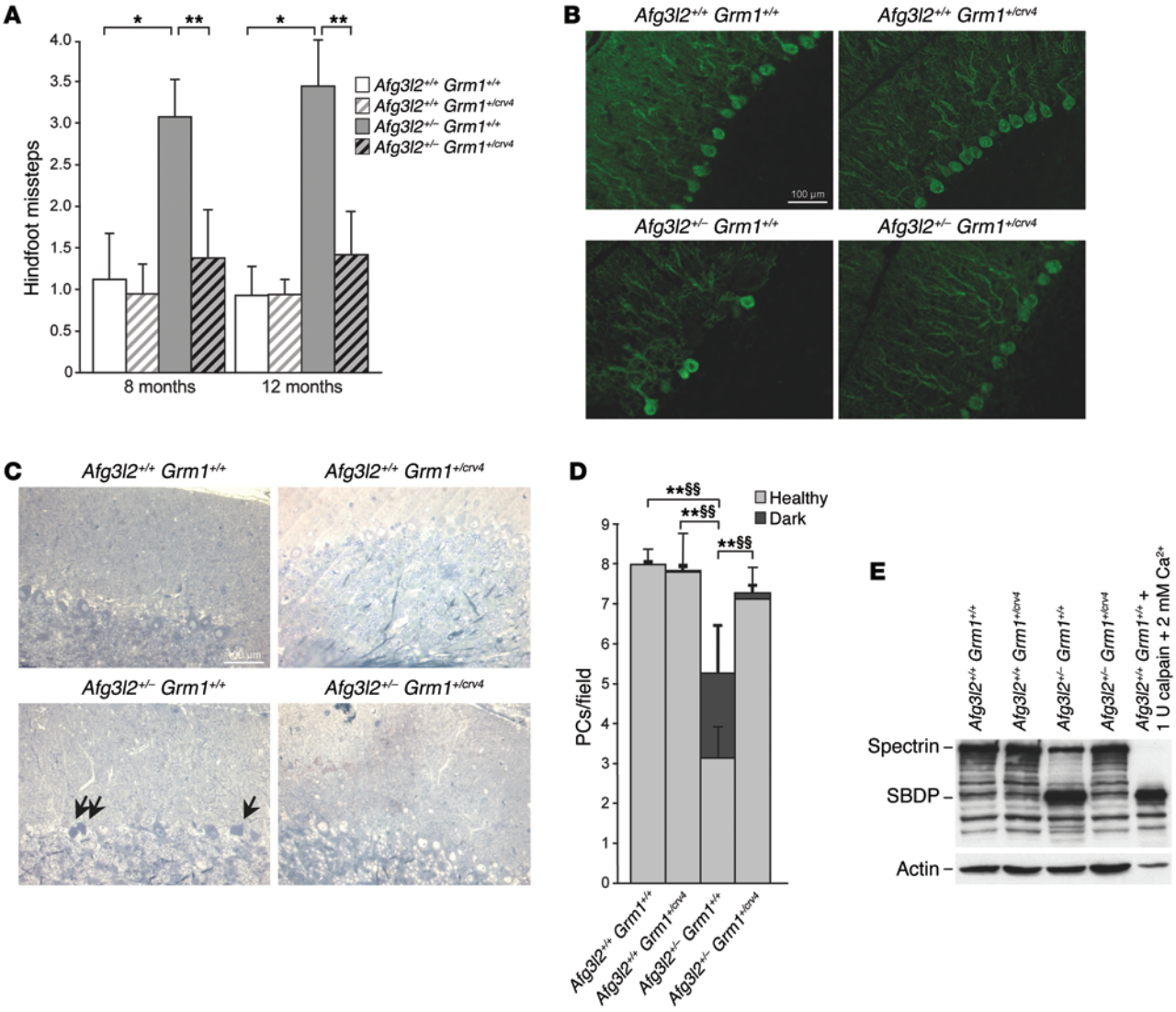

Figure 5. Half dosage of mGluR1 restores motor performances of Afg3l2$^{+/-}$ mice. (**A**) Beam-walking test performed on *Afg3l2*$^{+/-}$ *Grm1*$^{+/crv4}$ mice and their littermates at 8 and 12 months of age. Data represent the mean ± SD of 4 independent tests; n = 13–15. *$P < 0.05$ and **$P < 0.001$ by Student's t test. (**B**) Cryostat-cut sections of cerebellum from *Afg3l2*$^{+/-}$ *Grm1*$^{+/crv4}$ mice and their littermates at 8 months of age stained with anti-calbindin Ab. Scale bar: 100 μm.(**C**) Semithin sections of cerebellum from *Afg3l2*$^{+/-}$ *Grm1*$^{+/crv4}$ mice and their littermates at 8 months of age stained with toluidine blue. Arrows indicate dark PCs. (**D**) Quantification of healthy and dark PCs in 8-month-old *Afg3l2*$^{+/-}$ *Grm1*$^{+/crv4}$ mice. Data represent the mean ± SD; n = 4. $P < 0.001$ by Student's t test for both healthy (*) and dark (§) PCs. (**E**) WB analysis of cerebellar extracts from of *Afg3l2*$^{+/-}$ *Grm1*$^{+/crv4}$ mice and their littermates using anti-spectrin Ab. A cerebellar extract treated with 2 mM $CaCl_2$ and 1 U calpain was used as a positive control. Actin was used to verify equal loading.

tration markedly improved the motor capabilities of SCA28 mice. Indeed, the drug-treated mice made significantly fewer footslips in traversing the beam compared with saline-treated mutants at both 8 and 12 months of age (Figure 6A and Supplemental Video 3 and 4). This indicates that ceftriaxone treatment at presymptomatic stages is able to prevent, and not just delay, the ataxic phenotype in *Afg3l2*-haploinsufficient mice. In accordance with these findings, semithin sections of the cerebellum revealed a reduced number of PC-DCDs in treated *Afg3l2*$^{+/-}$ mice (Figure 6, B and C) that was also confirmed by WB, which showed an attenuation of calpain-mediated αII-spectrin cleavage (Figure 6D). Also, we found that PC numbers and dendritic tree arborization were completely recovered in the drug-treated mutants, as shown by IF using calbindin Ab (Figure 6B and Supplemental Figure 5B). Ceftriaxone treatment (as well as a halved dosage of mGluR1) produced neither adverse effects nor body-weight alterations, as demonstrated by the results of the SHIRPA (SmithKline Beecham, Harwell, Imperial College, Royal London Hospital, phenotype assessment) protocol (39), which revealed normal motor, sensory, autonomic, and neuropsychiatric functions (Supplemental Tables 1 and 2).

Of note, we demonstrated that ceftriaxone treatment is effective after onset of the ataxic phenotype. In fact, *Afg3l2*$^{+/-}$ mice treated at 8 and 10 months of age showed a significant amelioration of their motor coordination skills (Figure 6E and Supplemental Video 5 and 6).

The genetic and pharmacological rescues of the SCA28 phenotype were both based on the rationale that reducing Ca^{2+} influx into PCs could ameliorate DCD and ataxia in *Afg3l2*-haploinsuf-

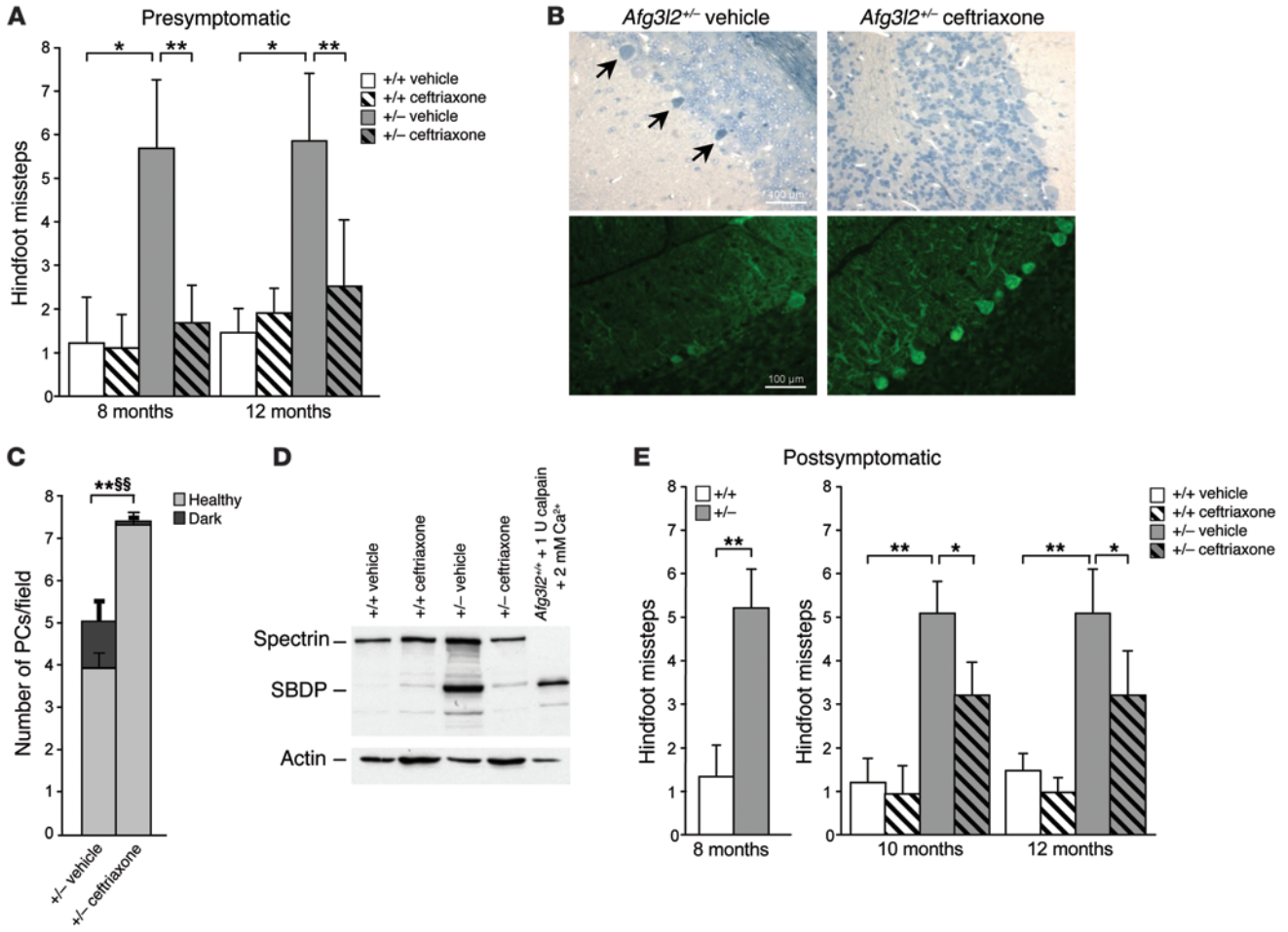

Figure 6. Presymptomatic treatment with ceftriaxone rescues both motor symptoms and PC-DCD in SCA28 mice. (**A**) Beam-walking test performed on *Afg3l2*$^{+/-}$ and WT mice treated with vehicle or ceftriaxone at presymptomatic stages. Data represent the mean ± SD of 4 independent tests; $n = 15$. *$P < 0.05$ and **$P < 0.001$ by Student's t test. (**B**) Semithin (upper panels) and cryostat-cut sections (lower panels) of cerebellum from ceftriaxone-treated versus vehicle-treated *Afg3l2*$^{+/-}$ and WT mice at 8 months of age stained with toluidine blue and anti-calbindin Abs, respectively. Arrows indicate dark PCs. Scale bars: 100 µm. (**C**) Quantification of healthy and dark PCs in ceftriaxone-treated versus vehicle-treated *Afg3l2*$^{+/-}$ mice. Data represent the mean ± SD; $n = 4$. $P < 0.001$ by Student's t test for both healthy (*) and dark (§) PCs. (**D**) WB analysis of cerebellar extracts from *Afg3l2*$^{+/-}$ and WT mice treated with vehicle or ceftriaxone using anti-spectrin Ab. A control cerebellar extract treated with 2 mM $CaCl_2$ and 1 U calpain was used as a positive control. (**E**) Beam-walking test performed on *Afg3l2*$^{+/-}$ mice and their littermates at postsymptomatic stages (8 months) and after ceftriaxone treatment. Data represent the mean ± SD of 4 independent tests; $n = 15$. *$P < 0.05$ and **$P < 0.001$ by Student's t test.

ficient mice. When designing this strategy, we were aware that by limiting the glutamatergic stimulation of PCs, we were intervening downstream of the primary pathological event at the mitochondrial level. Indeed, we interfered with the effects of impaired mitochondrial Ca^{2+} buffering on cytosolic Ca^{2+} concentrations. For this reason, it was expected that both genetic and pharmacologic interventions would have no effect on mitochondrial abnormalities, but we could not formally exclude the possibility. In fact, under physiological conditions, a limited Ca^{2+} increase stimulates mitochondrial metabolism. However, in the presence of an overriding pathological stimulus, Ca^{2+} concentrations have a detrimental effect on mitochondria, such as the stimulation of ROS production or induction of mitochondrial permeability transition (40). In order to test our hypothesis, we evaluated the possible amelioration of mitochondrial (a) morphological and (b) metabolic abnormalities in *Afg3l2*$^{+/-}$ *Grm1*$^{+/crv4}$ mice and in *Afg3l2*$^{+/-}$ mice treated with ceftriaxone compared with that in controls. EM analysis of cerebellar sections revealed no significant amelioration of mitochondrial morphology in *Afg3l2*$^{+/-}$ *Grm1*$^{+/crv4}$ mice compared with that seen in *Afg3l2*$^{+/-}$ mice (Supplemental Figure 6, A and B), nor was this observed in *Afg3l2*$^{+/-}$ mice treated with ceftriaxone compared with vehicle-treated *Afg3l2*$^{+/-}$ mice (Supplemental Figure 6, C and D). Also, EM study of primary PCs showed no amelioration of primary PC mitochondrial structures in *Afg3l2*$^{-/-}$ *Grm1*$^{+/crv4}$ mice compared with those observed in *Afg3l2*$^{-/-}$ mice in both basal conditions and after acute stimulation with DHPG (Supplemental Figure 6E).

We also performed a spectrophotometric assay of respiratory complex I activity on cerebellar protein extracts. As expected, we found a significant reduction in complex I activity in *Afg3l2*$^{+/-}$ mice compared with that in WT mice. However, this defect was not rescued in *Afg3l2*$^{+/-}$ *Grm1*$^{+/crv4}$ mice or in *Afg3l2*$^{+/-}$ mice treated with ceftriaxone, consistent with what we observed in the EM studies (Supplemental Figure 7, A and B).

These data indicate that the reduction of Ca^{2+} concentrations in PCs achieved by our interventions, while rescuing DCD and the clinical phenotype, was not able to recover the alterations in mitochondrial morphology and metabolism in SCA28 mice.

Discussion

In the present study, we provide evidence for a pathogenetic mechanism of SCA28 that involves defective mitochondrial Ca^{2+} buffering as a primary triggering event. The inefficient shaping of Ca^{2+} rises operated by mutant mitochondria upon stimulation results in a pathological increase in $[Ca^{2+}]_{cyto}$, which in turn triggers PC-DCD. Several data support this mechanism. First, we demonstrated in cerebellar slices treated with AMPA that *Afg3l2*$^{-/-}$ and *Afg3l2*$^{+/-}$ PCs are more prone to undergo DCD, indicating a reduced ability of mutant cells to cope with stimuli that increase $[Ca^{2+}]_{cyto}$.

We then determined that the increased sensitivity to high Ca^{2+} levels was due to reduced mitochondrial Ca^{2+} handling. We previously reported defective mitochondrial Ca^{2+} uptake in *Afg3l2*$^{-/-}$ fibroblasts, but this had no impact on cellular Ca^{2+} homeostasis (13), as is expected for nonexcitable and nonpolarized cells. We thus tested this hypothesis in primary PCs. The uniqueness of these neurons resides in their large soma and huge dendritic trees, which only receive glutamate excitatory synaptic input from a single climbing fiber and from approximately 200,000 parallel fibers. Thus, PCs require more precise control of Ca^{2+} homeostasis than do other neurons, implying greater Ca^{2+}-buffering power (27). These features suggest that mitochondrial Ca^{2+} buffering is crucial to PCs.

We directly measured $[Ca^{2+}]_{mito}$ in primary PCs after KCl induction and found it markedly reduced in *Afg3l2*$^{-/-}$ PCs. This defect had a marginal involvement in the maintenance of resting Ca^{2+} levels in PCs, since we determined that $[Ca^{2+}]_{cyto}$ was unchanged in *Afg3l2*$^{-/-}$ PCs under basal conditions. In contrast, we found that the evoked peak $[Ca^{2+}]_{cyto}$ response was markedly increased in *Afg3l2*$^{-/-}$ PCs, and this result perfectly matches the one obtained with treating control PCs with FCCP, which inhibits mitochondrial Ca^{2+} uptake. Of note, $[Ca^{2+}]_{cyto}$ pathological elevation in *Afg3l2*$^{-/-}$ PCs occurs not only in the presence of a depolarizing stimulus causing massive Ca^{2+} influx from the plasma membrane, but also in the presence of an mGluR1 agonist, which induces Ca^{2+} release from the ER. Previous studies showed that massive Ca^{2+} increases can be substantially buffered by mitochondria in other neuronal cell types, in which the addition of uncoupling agents results in a marked elevation of peak cytosolic Ca^{2+} levels (24–26). Our data, aside from elucidating the pathogenetic mechanism of SCA28, demonstrate for the first time to our knowledge the impact of defective mitochondrial Ca^{2+} uptake on local Ca^{2+} signaling in a physiopathological condition of the nervous system. This concept has been proposed as a potential pathogenetic mechanism of neurological disorders (27, 41) but has never been directly demonstrated and has thus far remained largely speculative.

We also demonstrated that reduced mitochondrial Ca^{2+} uptake capacity in *Afg3l2*-mutant PCs is the result of the negative synergy between alterations of mitochondrial morphology and impaired mitochondrial metabolism. Indeed, EM analysis revealed dramatic alterations of organellar ultrastructure in mutant PCs, showing mitochondria with vesiculation of the inner membrane or a completely swollen appearance. We observed aberrant organelles mainly in *Afg3l2*$^{-/-}$ PCs, but also in *Afg3l2*$^{+/-}$ PCs, indicating that *Afg3l2* haploinsufficiency is sufficient to exert mitochondrial damage in neuronal cells in vitro as well. In addition to these ultrastructural defects, *Afg3l2*$^{-/-}$ PCs showed increased mitochondrial network fragmentation and faulty mitochondrial distribution in the dendritic tracks. In particular, we observed that the mitochondrial volume associated with dendrites was reduced in the absence of AFG3L2, indicating a skewed distribution of mitochondria toward the cell soma.

AFG3L2 controls the morphology of the mitochondrial network via regulation of OPA1 processing. In particular, the absence of AFG3L2 causes increased mitochondrial fragmentation due to enhanced OPA1 processing (12, 13). Fragmentation of the mitochondrial network can modify organelle Ca^{2+} uptake by changing the interaction with the Ca^{2+} source (e.g., the ER and/or plasma membrane) and limiting proper diffusion of the Ca^{2+} wave along the mitochondrial network (42, 43). Indeed, this was the case in *Afg3l2*$^{-/-}$ fibroblasts (13).

Defects in both fusion and fission have been shown to affect mitochondrial movement (29). In *Afg3l2*$^{-/-}$ PCs, the increased diameter of mitochondria due to cristae disruption and swelling may hamper their efficient entry into dendrites, resulting in a lack of mitochondria in these processes. A similar situation was previously observed in mice in which mitofusin 2, a protein involved in mitochondrial fusion, was specifically ablated in PCs (44), indicating that these neurons are particularly sensitive to perturbations of mitochondrial dynamics.

In line with the morphological alterations, mitochondria in *Afg3l2*-mutant PCs were also metabolically dysfunctional, displaying reduced $\Delta\psi_{mito}$ in both soma and dendrites as a consequence of the respiratory chain defect we reported previously (9).

Thus, we propose a pathogenetic mechanism in which loss and haploinsufficiency of *Afg3l2* cause fragmentation and mild depolarization of mitochondria, which weakens mitochondrial buffering of Ca^{2+} elevations in the soma. This scenario is worsened in mutant dendrites due to underpopulation of mitochondria, too.

It is also conceivable that reduced ATP production by mutant mitochondria can locally slow down the kinetics of Ca^{2+} pumps, affecting extrusion of Ca^{2+} from the cytosol into the ER and across the plasma membrane in dendrites; however, this does not apply to the soma of PCs, in which the kinetics of Ca^{2+} recovery after stimulation is unaffected.

According to the proposed mechanism of neurodegeneration, the SCA28 phenotype is fully rescued by halving the amount of the mGluR1 receptor. The *Afg3l2*$^{+/-}$ *Grm1*$^{+/crv4}$ double mutants display motor function and coordination within the normal range, and degenerating PCs are remarkably reduced compared with those in *Afg3l2*$^{+/-}$ mice. Adult PCs express high levels of mGluR1 (but not mGluR5) in the soma and in dendritic spines, and this receptor is essential for synapse plasticity and motor coordination. Indeed, mice lacking mGluR1 display severe ataxia and deficits in spatial and associative learning (37, 45), and homozygous mutations in *GRM1* have been recently associated with a recessive form of congenital cerebellar ataxia (46).

Finally, we treated *Afg3l2*$^{+/-}$ mice with ceftriaxone, a safe and multipotent agent used for decades as an antimicrobial agent. This drug was shown to consistently increase the transcription levels of the astrocyte glutamate transporter EAAT2 (38).

On the basis of the SCA28 pathogenetic mechanism that we defined in this work, we used this drug to reduce the glutamatergic stimulation of PCs in *Afg3l2*$^{+/-}$ mice. We demonstrated that ceftriaxone treatment at both pre- and postsymptomatic stages was able to consistently reduce the number of PC-DCDs in the SCA28 model.

As expected, we found no amelioration of mitochondrial parameters in *Afg3l2*$^{+/-}$ mice treated with ceftriaxone or in *Afg3l2*$^{+/-}$ *Grm1*$^{+/crv4}$ double mutants. Indeed, our genetic and pharmacological interventions, by consistently reducing $[Ca^{2+}]_{cyto}$ and thus acting downstream of the primary insulting event at the mitochondrial level, were effective in rescuing DCD and the ataxic phenotype, but not the mitochondrial phenotypes. While further studies aimed at discovering therapies that specifically address SCA28 mitochondrial impairment are needed, administering ceftriaxone downstream in the pathogenic cascade is a potentially effective approach to treating additional forms of SCA that share the final stage of degeneration with SCA28 (i.e., elevated $[Ca^{2+}]_{cyto}$ in PCs).

The data presented in this work disclose important steps in the molecular pathogenesis of SCA28 and provide a strong rationale for a new approach to treating this disease. At present, effective therapies for cerebellar ataxias are lacking, although some improvements in ataxic and nonataxic symptoms have been reported in a few clinical trials (47). We believe our data will contribute to advancing therapeutics for patients with SCA28, as ceftriaxone is a widely used, well-tolerated antibiotic drug that represents an immediately available therapy for SCA28 patients as well as for those affected by other SCAs characterized by PC-DCD.

Methods

Animals, drug administration, and motor tests. *Afg3l2*$^{+/-}$ mice (16) were bred on an FVB/N background, and *Grm1*$^{+/crv4}$ mice were bred on a BALB/c/ background (37). In the genetic rescue experiments, *Afg3l2*$^{+/-}$ *Grm1*$^{+/crv4}$ mice and their littermates were bred on an FVB/N BALB/c/ mixed background. For the presymptomatic treatment, ceftriaxone (Sigma-Aldrich) was administered to 3-month-old mice by daily i.p. injection at a dose of 200 mg/kg body weight for 5 consecutive days (2 months before the onset of motor impairment in SCA28 mice; ref. 16). The treatment was repeated 2 months later. For the postsymptomatic treatment, ceftriaxone was administered to mice at 8 and 10 months of age by daily i.p. injection at a dose of 200 mg/kg body weight for 5 consecutive days. Beam-walking and SHIRPA tests were performed as previously described (16), and investigators were blinded to the treatment group during assessments.

Abs, drugs, and reagents. For WB analysis, commercially available monoclonal Abs were used for the detection of rabbit anti-GLT1 (PA3-040A; Thermo Scientific); mouse anti-spectrin (MAB1622; EMD Millipore); mouse anti–β-actin–peroxidase clone AC-15 (A3854; Sigma-Aldrich); and rat anti–PSD-95 (ab2723; Abcam). ECL anti-mouse and anti-rabbit IgG and HRP-linked species-specific whole Abs were purchased from GE Healthcare.

For IF experiments, the following Abs were used: rabbit anti–spectrin–breakdown product (anti-SBDP) (30, 31); mouse anti–GFAP clone G-A-5 (G3893; Santa Cruz Biotechnology Inc.); mouse anti–NeuN clone A60 (MAB377; EMD Millipore); rabbit anti–calbindin 28 kDa (300; Swant); and anti–OxPhos complex IV subunit I (A-6403; Invitrogen). Secondary Abs were conjugated with Alexa 488 and Alexa 596 (A11001 and A11010; Invitrogen).

WB analyses. Spectrin band patterns were analyzed by standard WB procedure. Briefly, tissues were homogenized in 50 mM Tris-HCl (pH 7.4), 5 mM EDTA, 1% Triton X-100, and 1 mM DTT using a glass-Teflon homogenizer and incubated for 90 minutes on ice. Cell debris was discarded by centrifugation at 8,000 *g* for 5 minutes at 4°C. Controls consisted of WT lysates treated with 100 μM or 2 mM $CaCl_2$ or 1 U recombinant rat calpain (EMD Millipore) for 30 minutes at 37°C.

For EAAT2 detection, synaptosomes were isolated as follows: mouse cerebellum was homogenized in sucrose buffer (320 mM sucrose, 5 mM HEPES [pH 7.4], and 2 mM EDTA) and a protease inhibitor cocktail (PIC) (Sigma-Aldrich) using a glass-Teflon homogenizer. Tissue debris was discarded by centrifugation at 1,000 *g* for 10 minutes at 4°C. Supernatants were centrifuged at 10,000 *g* for 15 minutes at 4°C, and the pellet was resuspended in 5 mM HEPES (pH 7.4) plus PIC, homogenized with a glass-Teflon homogenizer, incubated for 30 minutes on ice, and centrifuged at 20,000 *g* for 30 minutes at 4°C. The synaptosome pellet was resuspended in sucrose buffer and analyzed by WB.

Organotypic slices and PC primary cultures. Organotypic slices from cerebellum were prepared from P10 mice, as previously described (32). Cerebella were removed from newborn *Afg3l2* mice. Sagittal cerebellar sections (400-μm thickness) were cut using a chopper tissue slicer (McIlwaintissue Chopper; Stoelting Co.) and placed on Millicell-CM organotypic tissue–culture plate inserts (EMD Millipore) in a medium containing Basal Medium Eagle (Sigma-Aldrich), 25% horse serum (Invitrogen), 0.5% glucose, 2 mM GlutaMax (Invitrogen), 100 U/ml PenStrep (Invitrogen), and 2.5 μM arabinofuranosyl cytidine (Ara-C; Sigma-Aldrich). After 4 to 5 DIV, slices were exposed to 50 μM AMPA (Tocris) for 30 minutes. Controls consisted of identical manipulation for the entire experiment without AMPA. Slices were then fixed in 4% paraformaldehyde solution, transferred to a 10%–20%, and finally a 30%, sucrose solution and then frozen. Sections (16-μM thickness) were cryostat cut with a Leica CM1850.

For primary PC cultures, a modified version of previously described protocols (48) was used. Cerebella from newborn mice were incubated in HBSS 1X (Invitrogen) containing 5 U/ml papain (Sigma-Aldrich), 50 mg/ml cystein-HCl, 0.1 mM EDTA, and 1 mg/ml DNase I (EMD Millipore) for 30 minutes at 37°C. Tissues were then dissociated by mechanical trituration. The reaction was blocked with 10% horse serum, and samples were centrifuged at 100 *g* for 10 minutes. The cellular pellet was washed twice in HBSS 1X and resuspended in cultured medium containing Neurobasal (Invitrogen), B27 supplement (Invitrogen), 200 mg/ml D-glucose, 2 mM GlutaMax (Invitrogen), 100 U/ml PenStrep (Invitrogen), 1% horse serum (Invitrogen), 3 mM KCl, and 50 ng/ml NGF 2.5S (EMD Millipore). Cells were plated at a density of $1.5 \times 10^4/cm^2$ on coverslips (14 mm or 24 mm in diameter) or in glass-bottom culture dishes (MatTek) coated with Poly-L-Lysine (Sigma-Aldrich).

Measurement of $\Delta\psi_{mito}$. $\Delta\psi_{mito}$ was measured using the potentiometric dye TMRM (Invitrogen). Primary PCs at 14 DIV were incubated with 50 nM TMRM, 2 mM CsH (Vinci-Biochem), and 2 mg/ml Hoechst 33342 (Invitrogen) in phenol red–free HBSS 1× for 30 minutes at 37°C. Imaging of TMRM fluorescence was performed using an Axio Observer.Z1 inverted microscope (Zeiss). Data represent the average of 4 images acquired every 15 seconds. FCCP (1 μM) was added at the end of acquisition. Images were analyzed using ImageJ software (NIH).

Morphometric analyses of primary PCs. IF was performed on primary PCs at 14 DIV. Stacks of consecutive confocal images were taken

at 0.3-μm intervals using a PerkinElmer UltraVIEW Spinning Disk Confocal Microscope. Analyses of soma and dendrite area and total mitochondria volume were performed using Volocity 3D Image Analysis Software, version 5.5.1 (PerkinElmer). For mitochondrial volume evaluation, a region of interest (ROI) was drawn to cover the profile of each PC (or dendrites only). A threshold for the red signal (mitochondria) and green signal (PCs) was set in order to exclude the background. Mitochondria with a red signal intensity greater than or equal to the green threshold were identified as belonging to PCs. This analysis was extended to the whole cell volume.

Syn-4mtD1cpv rAd construction, production, and titering. 4mtD1cpv pcDNA3 was used as a template in a PCR with the following primers: forward, 5′-TTATCGAAATTAATACGACTCACGTGGAATTCGCCACCATGTCCGTCC-3′; reverse, 5′-CCGCCAGTGTGATGGATATCTGCAGAATTCTTA-3′. The forward primer was designed to introduce an EcoRI restriction site at the 5′ end of 4mtD1cpv and a Kozak sequence to improve translation efficiency. The PCR product was then cloned in the EcoRI site of the pDC511 syn BGH-polyA vector (49). This shuttle plasmid carries the 470-bp human synapsin promoter to guarantee neuron-specific expression of the chameleon probe.

Second-generation rAd was produced by transfecting E2T cells (50) with the genomic helper plasmid (Microbix Biosystems Inc.) that had been modified to contain the E2a deletion and the pDC511 syn 4mtD1cpv-BGH PolyA vector, as previously described (49). Preparation of a high-titer viral stock from crude lysate was performed as described by Ng and Graham (51). The titer was determined by limiting dilution to obtain 3.1×10^7 PFU/ml.

Ca^{2+} imaging. $[Ca^{2+}]_{cyto}$ measurements were performed as previously described (52). Fura-2 acetoxymethyl ester (Calbiochem, Merck KGaA) loading was performed at 37°C (4 μM, 40 minutes) in Krebs Ringer HEPES buffer (containing 5 mM KCl, 125 mM NaCl, 2 mM $CaCl_2$, 1.2 mM $MgSO_4$, 1.2 mM KH_2PO_4, 6 mM glucose, and 20 mM HEPES [pH 7.4]). When the K^+ concentration was increased in the solution, the concentration of Na^+ was adjusted to maintain isotonicity. Excitation wavelengths of 340 and 380 nm were used with an emission wavelength of 510 nm. The 340:380 fura-2 ratio was calculated as mean values within ROIs drawn in neuronal soma. The time course of the intensity ratio was analyzed by custom-written routines in MATLAB (The MathWorks Inc.): the code scans each response curve to find its maximum value and fits the subsequent decay with a monoexponential in order to quantify the amplitude of the response and the characteristic time of the decay. To generate the average responses showed in Figure 2G, the curves were first synchronized to the time of maximum fold change, corresponding to the onset of the Ca^{2+} response to KCl.

For fluorescence resonance energy transfer (FRET) experiments, PCs were transduced at 5 DIV with an MOI of 60 and imaged for Ca^{2+} measurement 72 hours after infection. The FRET data were acquired on a Leica TCS SP-5 DS confocal microscope equipped with a ×63 NA 1.4 oil-immersion objective lens (Leica Microsystems). The light of a 405-nm solid-state laser was used to excite CFP, and the fluorescence emission from both CFP and YFP was collected simultaneously using 2 separate detection channels (CFP, 470–505 nm and YFP, 525–600 nm, respectively). PCs were easily distinguished from granule cells and neurons, being markedly larger and more ramified. Time series of 100 frames were collected using an imaging time of 1.314 seconds per image. After approximately 20 images, 30 mM KCl was added to the imaging medium as described above to quantify the mitochondrial calcium response. The FRET signal was quantified by measuring the background-subtracted ratio between YFP and CFP channels on pixels corresponding to mitochondria.

EM analysis. The semithin and ultrathin sections from mouse tissues and primary PCs at 14 DIV were prepared as previously described (16).

Statistics. Results are reported as the mean ± SD or SEM. Most of the experiments were evaluated by a 2-tailed Student's *t* test. *P* values were adjusted for multiple testing by applying the Holm-Bonferroni method (53). A χ^2 test with 2 degrees of freedom was applied for analysis of the ultrastructure of mitochondria. Scores from SHIRPA analysis were analyzed by a nonparametric Mann-Whitney *U* test. Comparisons were considered statistically significant when *P* was less than 0.05.

Study approval. All experiments involving animals were performed in accordance with experimental protocols approved by the IACUC of the San Raffaele Scientific Institute.

Acknowledgments

This work was supported by the Italian Telethon Foundation (GGP12235); Fondazione Cariplo (2012 0646); Ministero Italiano dell'Università e della Ricerca (MIUR, 20108WT59Y 001); Associazione Italiana Sindromi Atassiche (AISA); and Max Planck Society (to S.M. Young Jr.). F. Maltecca is a recipient of a Young Investigator Award for SCA research from the National Ataxia Foundation (NAF); I. Drago is a recipient of an EMBO fellowship (ASTF 365.00-2010). We thank Tullio Pozzan and Laura Cassina for critical discussion, Diana Pendin for virus preparation, Laura Corti for histological technical assistance and management of mouse colonies, and Valeria Barili for technical support with cerebellar slice preparation. We thank Alessandro Ambrosi for his support with statistical analyses throughout the study.

Address correspondence to: Giorgio Casari, Vita-Salute San Raffaele University and San Raffaele Scientific Institute, Via Olgettina 58, 20132 Milan, Italy. Phone: 39.02.2643.3502; E-mail: casari.giorgio@hsr.it.

1. Cagnoli C, et al. SCA28, a novel form of autosomal dominant cerebellar ataxia on chromosome 18p11.22-q11.2. *Brain*. 2006;129(pt 1):235–242.
2. Di Bella D, et al. Mutations in the mitochondrial protease gene AFG3L2 cause dominant hereditary ataxia SCA28. *Nat Genet*. 2010;42(4):313–321.
3. Cagnoli C, et al. Missense mutations in the AFG3L2 proteolytic domain account for approximately 1.5% of European autosomal dominant cerebellar ataxias. *Hum Mutat*. 2010;31(10):1117–1124.
4. Edener U, et al. Early onset and slow progression of SCA28, a rare dominant ataxia in a large four-generation family with a novel AFG3L2 mutation. *Eur J Hum Genet*. 2010;18(8):965–968.
5. Pierson TM, et al. Whole-exome sequencing identifies homozygous AFG3L2 mutations in a spastic ataxia-neuropathy syndrome linked to mitochondrial m-AAA proteases. *PLoS Genet*. 2011;7(10):e1002325.
6. Koppen M, Langer T. Protein degradation within mitochondria: versatile activities of AAA proteases and other peptidases. *Crit Rev Biochem Mol Biol*. 2007;42(3):221–242.
7. Arlt H, Steglich G, Perryman R, Guiard B, Neupert W, Langer T. The formation of respiratory chain complexes in mitochondria is under the proteolytic control of the m-AAA protease. *EMBO J*. 1998;17(16):4837–4847.
8. Atorino L, et al. Loss of m-AAA protease in mitochondria causes complex I deficiency and increased sensitivity to oxidative stress in hereditary spastic paraplegia. *J Cell Biol*. 2003;163(4):777–787.

9. Maltecca F, et al. The mitochondrial protease AFG3L2 is essential for axonal development. *J Neurosci*. 2008;28(11):2827–2836.
10. Ishihara N, Fujita Y, Oka T, Mihara K. Regulation of mitochondrial morphology through proteolytic cleavage of OPA1. *EMBO J*. 2006;25(13):2966–2977.
11. Duvezin-Caubet S, et al. OPA1 processing reconstituted in yeast depends on the subunit composition of the m-AAA protease in mitochondria. *Mol Biol Cell*. 2007;18(9):3582–3590.
12. Ehses S, et al. Regulation of OPA1 processing and mitochondrial fusion by m-AAA protease isoenzymes and OMA1. *J Cell Biol*. 2009;187(7):1023–1036.
13. Maltecca F, et al. Respiratory dysfunction by AFG3L2 deficiency causes decreased mitochondrial calcium uptake via organellar network fragmentation. *Hum Mol Genet*. 2012;21(17):3858–3870.
14. Nolden M, Ehses S, Koppen M, Bernacchia A, Rugarli EI, Langer T. The m-AAA protease defective in hereditary spastic paraplegia controls ribosome assembly in mitochondria. *Cell*. 2005;123(2):277–289.
15. Smets K, et al. Partial deletion of AFG3L2 causing spinocerebellar ataxia type 28. *Neurology*. 2014;82(23):2092–2100.
16. Maltecca F, Magnoni R, Cerri F, Cox GA, Quattrini A, Casari G. Haploinsufficiency of AFG3L2, the gene responsible for spinocerebellar ataxia type 28, causes mitochondria-mediated Purkinje cell dark degeneration. *J Neurosci*. 2009;29(29):9244–9254.
17. Leist M, Jaattela M. Four deaths and a funeral: from caspases to alternative mechanisms. *Nat Rev Mol Cell Biol*. 2001;2(8):589–598.
18. Ikeda Y, et al. Spectrin mutations cause spinocerebellar ataxia type 5. *Nat Genet*. 2006;38(2):184–190.
19. Custer SK, et al. Bergmann glia expression of polyglutamine-expanded ataxin-7 produces neurodegeneration by impairing glutamate transport. *Nat Neurosci*. 2006;9(10):1302–1311.
20. Kasumu A, Bezprozvanny I. Deranged calcium signaling in Purkinje cells and pathogenesis in spinocerebellar ataxia 2 (SCA2) and other ataxias. *Cerebellum*. 2012;11(3):630–639.
21. Ito M. The molecular organization of cerebellar long-term depression. *Nat Rev*. 2002;3(11):896–902.
22. Gruol D, Manto M, Haines D. Ca^{2+} signaling in cerebellar Purkinje neurons — editorial. *Cerebellum*. 2012;11(3):605–608.
23. Pizzo P, Drago I, Filadi R, Pozzan T. Mitochondrial Ca(2)(+) homeostasis: mechanism, role, and tissue specificities. *Pflugers Arch*. 2012;464(1):3–17.
24. Colegrove SL, Albrecht MA, Friel DD. Dissection of mitochondrial Ca^{2+} uptake and release fluxes in situ after depolarization-evoked [Ca2+](i) elevations in sympathetic neurons. *J Gen Physiol*. 2000;115(3):351–370.
25. David G, Barrett EF. Stimulation-evoked increases in cytosolic [Ca(2+)] in mouse motor nerve terminals are limited by mitochondrial uptake and are temperature-dependent. *J Neurosci*. 2000;20(19):7290–7296.
26. Montero M, et al. Control of secretion by mitochondria depends on the size of the local [Ca2+] after chromaffin cell stimulation. *Eur J Neurosci*. 2001;13(12):2247–2254.
27. Duchen MR. Mitochondria, calcium-dependent neuronal death and neurodegenerative disease. *Pflugers Arch*. 2012;464(1):111–121.
28. Corrado M, Scorrano L, Campello S. Mitochondrial dynamics in cancer and neurodegenerative and neuroinflammatory diseases. *Int J Cell Biol*. 2012;2012:729290.
29. Chen H, Chan DC. Mitochondrial dynamics — fusion, fission, movement, and mitophagy — in neurodegenerative diseases. *Hum Mol Genet*. 2009;18(R2):R169–R176.
30. Bahr BA, Tiriveedhi S, Park GY, Lynch G. Induction of calpain-mediated spectrin fragments by pathogenic treatments in long-term hippocampal slices. *J Pharmacol Exp Ther*. 1995;273(2):902–908.
31. Bahr BA, et al. Survival signaling and selective neuroprotection through glutamatergic transmission. *Exp Neurol*. 2002;174(1):37–47.
32. Mansouri B, et al. Involvement of calpain in AMPA-induced toxicity to rat cerebellar Purkinje neurons. *Eur J Pharmacol*. 2007;557(2–3):106–114.
33. Czogalla A, Sikorski AF. Spectrin and calpain: a 'target' and a 'sniper' in the pathology of neuronal cells. *Cell Mol Life Sci*. 2005;62(17):1913–1924.
34. Strahlendorf JC, Acosta S, Strahlendorf HK. Diazoxide and cyclothiazide convert AMPA-induced dark cell degeneration of Purkinje cells to edematous damage in the cerebellar slice. *Brain Res*. 1996;729(2):197–204.
35. Baptista CA, Hatten ME, Blazeski R, Mason CA. Cell-cell interactions influence survival and differentiation of purified Purkinje cells in vitro. *Neuron*. 1994;12(2):243–260.
36. Palmer AE, et al. Ca^{2+} indicators based on computationally redesigned calmodulin-peptide pairs. *Chem Biol*. 2006;13(5):521–530.
37. Conti V, et al. crv4, a mouse model for human ataxia associated with kyphoscoliosis caused by an mRNA splicing mutation of the metabotropic glutamate receptor 1 (Grm1). *Int J Mol Med*. 2006;18(4):593–600.
38. Rothstein JD, et al. β-Lactam antibiotics offer neuroprotection by increasing glutamate transporter expression. *Nature*. 2005;433(7021):73–77.
39. Irwin S, Banuazizi A, Kalsner S, Curtis A. One trial learning in the mouse. I. Its characteristics and modification by experimental-seasonal variables. *Psychopharmacologia*. 1968;12(4):286–302.
40. Brookes PS, Yoon Y, Robotham JL, Anders MW, Sheu SS. Calcium, ATP, and ROS: a mitochondrial love-hate triangle. *Am J Physiol Cell Physiol*. 2004;287(4):C817–C833.
41. Barrett EF, Barrett JN, David G. Mitochondria in motor nerve terminals: function in health and in mutant superoxide dismutase 1 mouse models of familial ALS. *J Bioenerg Biomembr*. 2011;43(6):581–586.
42. Frieden M, James D, Castelbou C, Danckaert A, Martinou JC, Demaurex N. Ca(2+) homeostasis during mitochondrial fragmentation and perinuclear clustering induced by hFis1. *J Biol Chem*. 2004;279(21):22704–22714.
43. Szabadkai G, Simoni AM, Chami M, Wieckowski MR, Youle RJ, Rizzuto R. Drp-1-dependent division of the mitochondrial network blocks intraorganellar Ca^{2+} waves and protects against Ca^{2+}-mediated apoptosis. *Mol Cell*. 2004;16(1):59–68.
44. Chen H, McCaffery JM, Chan DC. Mitochondrial fusion protects against neurodegeneration in the cerebellum. *Cell*. 2007;130(3):548–562.
45. Ichise T, et al. mGluR1 in cerebellar Purkinje cells essential for long-term depression, synapse elimination, and motor coordination. *Science*. 2000;288(5472):1832–1835.
46. Guergueltcheva V, et al. Autosomal-recessive congenital cerebellar ataxia is caused by mutations in metabotropic glutamate receptor 1. *Am J Hum Genet*. 2012;91(3):553–564.
47. Matilla-Duenas A. Machado-Joseph disease and other rare spinocerebellar ataxias. *Adv Exp Med Biol*. 2012;724:172–188.
48. Tabata T, Sawada S, Araki K, Bono Y, Furuya S, Kano M. A reliable method for culture of dissociated mouse cerebellar cells enriched for Purkinje neurons. *J Neurosci Methods*. 2000;104(1):45–53.
49. Montesinos MS, Chen Z, Young SM Jr. pUNISHER: a high-level expression cassette for use with recombinant viral vectors for rapid and long term in vivo neuronal expression in the CNS. *J Neurophysiol*. 2011;106(6):3230–3244.
50. Zhou H, Beaudet AL. A new vector system with inducible E2a cell line for production of higher titer and safer adenoviral vectors. *Virology*. 2000;275(2):348–357.
51. Ng P, Graham FL. Construction of first-generation adenoviral vectors. *Methods Mol Med*. 2002;69:389–414.
52. Codazzi F, et al. Synergistic control of protein kinase Cgamma activity by ionotropic and metabotropic glutamate receptor inputs in hippocampal neurons. *J Neurosci*. 2006;26(13):3404–3411.
53. Holm S. A simple sequentially rejective multiple test procedure. *Scand J Statist*. 1979;6:65–70.